Geological Survey
of Canada


# Current Research
# 2000-E15

# *Shale permeability and pore-structure evolution characteristics*

***T.J. Katsube***

**2000**

Natural Resources Canada  Ressources naturelles Canada

Canada

Catalogue No. M44-2000/E15E-IN
ISBN 0-660-18220-3

Available in Canada from the
Geological Survey of Canada Bookstore website at:
http://www.nrcan.gc.ca/gsc/bookstore (Toll-free: 1-888-252-4301)

A copy of this publication is also available for reference by depository libraries across Canada through access to the Depository Services Program's website at http://dsp-psd.pwgsc.gc.ca

Price subject to change without notice



## Author's address

***T.J. Katsube*** *(jkatsube@nrcan.gc.ca)*
*Mineral Resources Division*
*Geological Survey of Canada*
*601 Booth Street*
*Ottawa, Ontario K1A 0E8*

# Shale permeability and pore-structure evolution characteristics

T. John Katsube

Mineral Resources Division, Ottawa

*Katsube, T.J., 2000: Shale permeability and pore-structure evolution characteristics; Geological Survey of Canada, Current Research 2000-E15; 9 p. (online; http://www.nrcan.gc.ca/gsc/bookstore)*

---

**Abstract:** Evolution characteristics of shale pore-structure components (e.g. storage and connecting pores) with compaction have been determined, for the first time, using several types of shale and mudstone samples in order to generate data for use in analyzing overpressure detection problems. Discrepancies between overpressure responses from different geophysical logs have been reported, suggesting that some logs may respond only to specific components.

Results indicate that, although some theoretical problems still exist, evolution characteristics can be successfully determined, separately, for shale storage and connecting pores. They indicate that storage porosities are generally constant but that connecting porosities always decrease with increased pressure, implying that connecting pores are more flexible and susceptible to pore-pressure changes. This may explain some of the reasons for log response discrepancies to overpressure.

**Résumé :** Les caractéristiques de l'évolution des composantes de la structure des pores du shale (p. ex. pores de stockage et de raccordement) en fonction de la compaction ont été déterminées pour la première fois en utilisant plusieurs types d'échantillons de shale et de mudstone. Ces déterminations ont été effectuées afin d'obtenir des données à utiliser dans l'analyse des problèmes de détection de surpression. Des différences dans les réponses à la surpression ont été signalées pour différentes diagraphies géophysiques, ce qui fait penser que certaines diagraphies peuvent n'être sensibles qu'à certaines composantes spécifiques.

Bien que persistent encore certains problèmes théoriques, les résultats indiquent que les caractéristiques de l'évolution peuvent être déterminées séparément avec succès pour les pores de stockage et les pores de raccordement dans le shale. On observe que les porosités de stockage sont relativement constantes, mais que les porosités de raccordement diminuent toujours en fonction d'une pression accrue, ce qui laisse penser que les pores de raccordement sont davantage déformables et sensibles à des variations de la pression interstitielle. Cela pourrait en partie expliquer les différences observées dans les diagraphies quant aux réponses à la surpression.

## INTRODUCTION

Evolution characteristics for a set of shale pore-structure components (storage porosity, connecting porosity, flow-path size, and flow-path density) with compaction have been determined, for the first time, to generate information for use in analysis of problems related to fluid expulsion and entrapment in shales, such as overpressure detection. This has been achieved by deriving the pore-structure component data from bulk petrophysical data (permeability, porosity, and formation factor as a function of increased pressure) that has been reported (Loman et al., 1993; Katsube and Coyner, 1994; Katsube and Williamson, 1994, 1998; Katsube et al., 1996a, b, 1999a, b; Katsube and Connell, 1998) for seven shale and mudstone samples.

Recent studies (Hermanrud et al., 1998, 1999) report discrepancies between the way that different logs run in a North Sea shale responded to overpressure, and suggest that this is due to some geophysical logs responding to bulk shale porosities and others to only the fracture sections of the interconnected pore system. This is a subject related to the fluid expulsion characteristics of the pore-structure components. Another study (Katsube et al., 1999a) suggested that in a storage-connecting pore system, significant porosity reduction may occur at great depth (>3.0 km) even after shale has reached a state of maximum compaction, but that some logs may respond only to changes in the sizes and shapes of the connecting pores. Although, considerable knowledge exists on shale compaction (e.g. Hedburg, 1936; Magara, 1980), which is to some extent reviewed in Hinch (1980), little knowledge exists on the evolution of individual pore-structure components during compaction. The purpose of this paper is to present new data on the evolution characteristics of pore-structure components, and to document the methods used to derive these data.

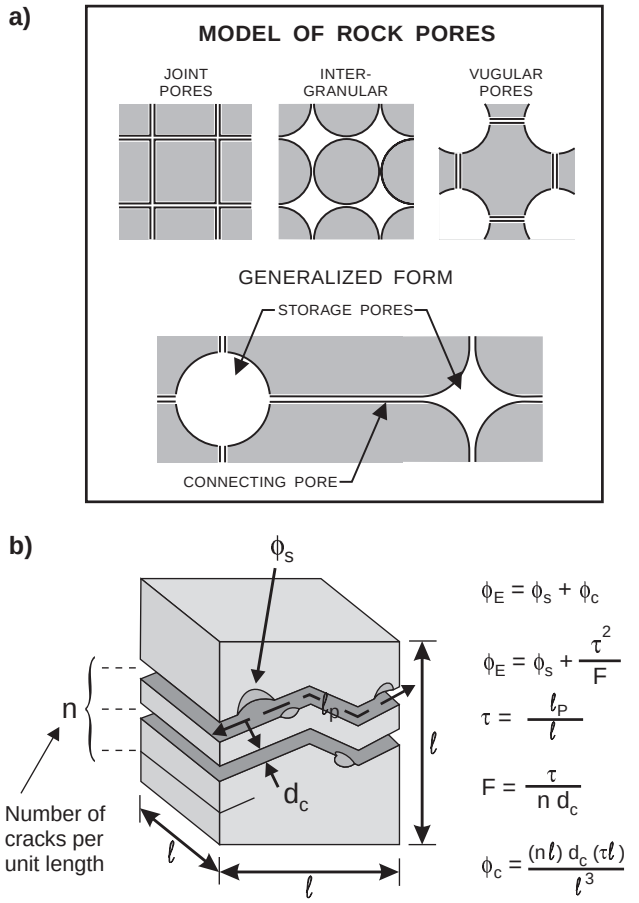


***Figure 1.*** *Two pore structure models used for characterizing shale (Katsube and Williamson, 1994):* ***a)*** *storage-connecting pore model (Katsube and Collett, 1975), and* ***b)*** *tortuous connecting and pocket pore model (Katsube and Kamineni, 1983).*

## BASIC PORE STRUCTURE AND THEORY

### *Pore-structure models*

There are three models (Katsube and Mareschal, 1993; Katsube and Williamson, 1994, 1998) that have proven to be very useful in describing shale pore-structure characteristics. The 'storage-connecting pore model' (Fig. 1a) describes the two basic types of storage pores (intergranular and vugular) and which are interconnected by connecting pores. The 'tortuous connecting pore model' (Fig. 1b) describes the tortuous nature of sheet-like connecting pores. This represents only one set of three orthogonal tortuous sheet-like parallel pore sets which are more descriptive of an actual isotropic rock (Katsube et al., 1991). The 'pore-size distribution model' describes the variation in connecting pore sizes, with Figure 2b representing a typical pore-size distribution of a tight shale. Pore-size distribution is derived from mercury intrusion-extrusion porosimetry. The typical set of mercury intrusion-extrusion curves in Figure 2a (Wardlaw and Taylor, 1976) show a difference between the mercury intruded volume at maximum intrusion pressure and the mercury extruded volume, leaving residual mercury in the sample after that pressure has been removed. This provides proof that storage pores exist.

### *Pore-structure parameters and theory*

The effective porosity ($\phi_E$) represents the pore space in all interconnected pores, and based on the 'storage-connecting pore model' (Fig. 1a), it is expressed by

$$\phi_E = \phi_S + \phi_C, \qquad (1)$$

where $\phi_S$ and $\phi_C$ are the storage and connecting porosities, respectively. Based on the 'tortuous connecting pore mode' (Fig. 1b), $\phi_C$ is defined by (Katsube and Williamson, 1994)

$$\phi_C = \tau n_C d_C = \tau n_{C0} (d_C/2)^2 \pi, \qquad (2)$$

where $\tau$ and $d_C$ are the tortuosity and flow-path size, respectively, and $n_C$ and $n_{CO}$ are the flow-path densities for sheet-like and tubular connecting pores, respectively. The units for $n_C$ and $n_{CO}$ are sheet-like and tubular connecting

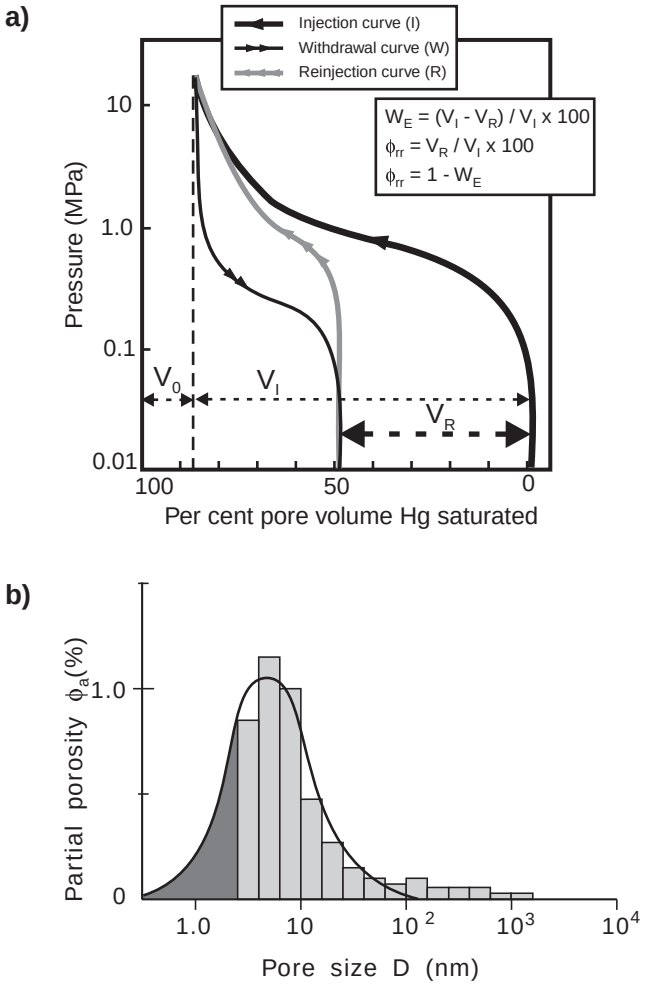


***Figure 2.*** *Diagrams* ***a)*** *describing the mercury intrusion and extrusion curves (*modified from *Wardlaw and Taylor, 1976), which form the basis of the* ***b)*** *pore-size distribution model (Katsube, 1992). $V_I$, $V_R$, and $V_0$ are the total mercury intrusion and residual volumes, and the volume of pore space not intruded by mercury, respectively. The $\phi_a$ is partial porosity, and d is the general expression for pore sizes.*

pores per unit volume. This equation represents the connecting pore sets in all three orthogonal directions. The $\tau$ is the actual flow-path length over the spatial distance between two points in a connecting pore (Fig. 1b), and is unity for the 'storage-connecting pore model' (Fig. 1a) because of its simplified connecting pore system. A larger value of 3.3 was obtained for an actual set of shale samples (Katsube et al., 1991).

The formation factor (F) and permeability (k) represent flow-path characteristics and are expressed by

$$F = b_1\tau/n_C d_C = b_1\tau^2/\phi_C, \quad (3)$$

where $b_1$ is a coefficient equal to 1.5 for sheet-like (Katsube et al., 1991) and to 3.0 for tubular pores, and by

$$k = d_C^2/(b_0 F), \quad (4)$$

where $b_0$ is a coefficient equal to 12 for sheet-like pores and to 8 for tubular pores (Walsh and Brace, 1984). Whereas Equation (2) represents connecting pores in all three orthogonal directions, Equations (3) and (4) consider that only two of the sheet-like connecting pore sets or one of the tubular connecting pore sets contribute to the flow of electrical current and fluid along a principal flow direction. All connecting pores are considered to be sheet-like in this study ($b_1 = 1.5$, $b_0 = 12$). The flow-path size ($d_C$) is derived from (Walsh and Brace, 1984)

$$d_C = \sqrt{(b_0 F k)}, \quad (5)$$

and represents the thickness or diameter of the flow paths. Flow paths, implies connecting pores that contribute to the transport of fluids, chemical species, or electrical current through a geological formation, and are distinguished from blind, dead-end, or storage pores of the interconnected pore network. Storage pores include all types of dead-end pores (e.g. Katsube, 1981) connected to the interconnected pore network, but do not contribute to the migration of fluids through the rock formations.

## ANALYTICAL APPROACH

### *Theoretical approach*

Out of the seven pore-structure parameters previously discussed, three are directly measured — effective porosity ($\phi_E$), permeability (k), and formation factor (F). The remaining four — storage porosity ($\phi_S$), connecting porosity ($\phi_C$), flow-path size ($d_C$), and flow-path density ($n_C$), are derived from these three, using Equations (1) to (5). At this point, $d_C$ can be directly derived from k and F using Equation (5), but the rest ($\phi_C$, $\phi_S$, $n_C$) require that $\tau$ be known (Equations (2) to (4)). In this study, $\tau$ is determined, statistically, from sets of $\phi_E$ and F measurements made at different effective pressures ($P_E$) on each sample, using the following equation (Katsube et al., 1991):

$$\phi_E = \phi_S + b_1\tau^2/F, \quad (6)$$

which can also be derived from Equations (1) and (3). Once $\tau$ is known, $\phi_C$ and $n_C$ are derived from Equation (3), and $\phi_S$ from Equation (1).

### *Permeability, effective-porosity, and formation-factor data*

The k, $\phi_E$, and F values at different effective pressures ($P_E$, 0–52 MPa) for the seven samples used in this study are listed in Tables 2a and 2b (*see* below), and have been derived from published data (e.g. Loman et al., 1993; Katsube and Coyner, 1994; Katsube et al., 1996a, b). The $\phi_E$ data in these tables (column 3) were obtained directly from the literature. The F data (column 5) were converted from the apparent formation-factor ($F_a$) data in the literature, using a newly developed technique (Katsube, 1999). This is a simple low-cost technique that eliminates the pore-surface conductivity effect

**Table 1.** Sample information for those used in this study, with references to original documents containing further details.

| Sample | Depth (km) | Basin | Rock type | Diagenesis | Epoch | Reference |
|---|---|---|---|---|---|---|
| V-4 | 4.96 | SB | Shale | Altered-DS | Jurassic | Katsube and Williamson, 1994 |
| V-7 | 5.27 | SB | Siltstone | Altered-DS | Jurassic | Katsube and Williamson, 1994 |
| V-8 | 5.27 | SB | Sandstone | Altered-DS | Jurassic | Katsube and Williamson, 1994 |
| V-9 | 5.55 | SB | Shale | Altered-CM | Jurassic | Katsube and Williamson, 1994 |
| TG-B | 2.46 | BMB | Shale | Unaltered | Tertiary | Issler and Katsube, 1994<br>Bloch and Issler, 1996 |
| EJA-2 | 0.896 | BMB | Mudstone | Unaltered | Tertiary | Katsube et al., 1999a |
| VSF-1 | SF | SB | Mud | Unaltered | | Katsube and Coyner, 1994<br>Katsube et al., 1996a, b |

SF=Seafloor, SB=Sable Basin, offshore Nova Scotia, BMB=Beaufort Mackenzie Basin, northern Canada, DS=Advanced stage of diagenetic dissolution, CM=Advanced stage of diagenetic cementation

from the $F_a$-$P_E$ data. The $\phi_E$ and $F_a$ measurements were made simultaneously at identical pressures (e.g. Loman et al., 1993). Samples used for these measurements, including the k measurements, were usually obtained from one inch plugs taken from 4 inch (101.6 mm) split-core samples from various wells in North America (e.g. Katsube et al., 1991). The source of the data used in this study are listed in Table 1. Several disc specimens, 0.5–1.5 cm in thickness, were cut from each of these plugs for the k-$P_E$ and the $F/\phi_E$-$P_E$ measurements. Cuttings, disks or partial disk specimens from the same samples were used for the other measurements (e.g. helium and mercury porosity, shale texture including scanning electron microscopy, and X-ray diffraction).

The k measurements were made on different specimens at different $P_E$ values from those of the $F/\phi_E$-$P_E$ measurements. For this reason, the k-$P_E$ data have been curve-fitted using the following equation,

$$k = k_o \exp(-\alpha P_e), \qquad (7)$$

and the coefficients ($k_0$, $\alpha$) determined (e.g. Katsube and Coyner, 1994). A one to two curve system has been used in this study, implying a maximum of two sets of coefficients ($k_{01}$, $\alpha_1$, $k_{02}$, $\alpha_2$) for each sample. Using these values and Equation (7), new k values were determined (column 4) at $P_E$ values identical to those of the $F/\phi_E$-$P_E$ measurements. The confining pressures ($P_C$) values for the $\phi_E$ and F data, in the literature, are equated to $P_E$ of the k data. This is because, the $F/\phi_E$-$P_E$ measurements were run with the pore-fluid pressure vented to the atmosphere. These low-k measurements were made by use of the pulse-transient decay technique (Brace et al., 1968; Coyner et al., 1993).

### *Selection of shale and mudstone samples*

Three shale samples V-8, V-7, and B-TG-6 (Tables 1, 2a, 2b) were selected to represent the three shale k-$P_E$ characteristic groups previously reported (Katsube and Connell, 1998); AA ($10^{-20}$–$1.6\times10^{-18}$ m²), BB ($10^{-22}$–$10^{-19}$ m²), and CC ($3\times10^{-23}$–$1.6\times10^{-18}$ m²), respectively. Samples V-9 and V-4 are diagenetically altered shale, and have been selected to represent typical shale at advanced stages of cementation and dissolution, respectively. Whereas the preceding five samples are from depth greater than 2.4 km, depth at which the state of maximum compaction is usually achieved (Katsube and Williamson, 1998), samples EJA-2 (0.896 km) and VSF-1 (seafloor) are unaltered mudstone and loose sediments representing material from shallower depth. Published data for only 1–7 MPa has been used in this study for sample VSF-1, in order to investigate the early stages of seafloor mud being compacted for the first time. Curve fitting has been used to determine the $\phi_E$, k, and F values at the required pressures for this sample, because the pressure ranges and the pressures at which the k and the $\phi_E$ and F measurements were made vary considerably.

## ANALYTICAL RESULTS

Effective porosity ($\phi_E$), permeability (k), and formation factor (F) as a function of effective pressure ($P_E$) for the seven shale, mudstone, and seafloor samples are plotted in Figure 3, using the data in Tables 2a and 2b. These show considerable decrease for k, a slight decrease for $\phi_E$ with the exception of the seafloor sample (VSF-1), and an increase for F with increased $P_E$ values. These trends are typical of those already published (e.g. Katsube and Williamson, 1994, 1998; Katsube et al., 1996a, b).

The $\phi_E$ -1/F curves are displayed in Figure 4 for all seven samples. These curves were interpreted to be linear, and used to determine the tortuosity ($\tau$) values (Equation (6)). The storage porosity determined by this method is represented by $\phi_{ST}$, in order to distinguish it from the storage porosity ($\phi_S$) derived from Equations (1) and (3). The results for $\tau$ and $\phi_{ST}$ are listed in Tables 2a and 2b (column 1). The results of all of the derived parameters, $\phi_S$, connecting porosity ($\phi_C$), flow-path size ($d_C$), and flow-path density ($n_C$) are listed in Tables 2a and 2b (columns 6–9), and displayed in Figure 5 for $\phi_S$ and $\phi_C$ and in Figure 6 for $d_C$ and $n_C$.

**Table 2a.** Measured (k, $\phi_E$, F) and derived ($\phi_S$, $\phi_C$, $d_C$, $n_C$) parameters for four shale samples from the Sable Basin, offshore Nova Scotia (Katsube and Williamson, 1994).

| Sample | $P_E$ (MPa) | $\phi_E$ (%) | k ($x10^{-21} m^2$) | F | $\phi_S$ (%) | $\phi_C$ (%) | $d_C$ (nm) | $n_C$ ($/m^2$) |
|---|---|---|---|---|---|---|---|---|
| **V-4** | 3.5 | 4.7 | 42.5 | 405 | 1.4 | 3.33 | 14.4 | $7.7x10^5$ |
| | 6.9 | 3.4 | 32.4 | 536 | 0.88 | 2.52 | 14.4 | $5.8x10^5$ |
| $\tau/\phi_{ST}$=3.0/0.4 | 13.8 | 2.1 | 18.6 | 793 | 0.40 | 1.70 | 13.3 | $4.3x10^5$ |
| $k_{01}/\alpha_1$=56/0.08 | 27.6 | 1.05 | 6.19 | 1610 | 0.21 | 0.84 | 10.9 | $2.6x10^5$ |
| | 34.5 | 0.78 | 3.56 | 2290 | 0.19 | 0.59 | 9.89 | $2.0x10^5$ |
| | 51.7 | 0.26 | 0.901 | 6880 | 0.064 | 0.20 | 8.62 | $7.6x10^4$ |
| **V-7** | 3.5 | 7.2 | 17.5 | 590 | 6.7 | 0.54 | 11.1 | $3.3x10^5$ |
| | 6.9 | 7.2 | 11.7 | 671 | 6.7 | 0.48 | 9.72 | $3.4x10^5$ |
| $\tau/\phi_{ST}$=1.5/6.7 | 13.8 | 7.1 | 5.24 | 831 | 6.7 | 0.39 | 7.23 | $3.6x10^5$ |
| $k_{01}/\alpha_1$=26/0.117 | 27.6 | 7.0 | 1.33 | 1150 | 6.7 | 0.28 | 4.28 | $4.5x10^5$ |
| $k_{02}/\alpha_2$=4.6/0.045 | 34.5 | 6.9 | 0.975 | 1670 | 6.7 | 0.19 | 4.42 | $3.0x10^5$ |
| | 51.7 | 6.8 | 0.450 | 2510 | 6.7 | 0.13 | 3.68 | $2.4x10^5$ |
| **V-8** | 3.5 | 7.7 | 55.4 | 420 | 5.9 | 1.84 | 16.7 | $4.8x10^5$ |
| | 6.9 | 7.4 | 49.7 | 460 | 5.7 | 1.68 | 16.6 | $4.5x10^5$ |
| $\tau/\phi_{ST}$=2.3/5.8 | 13.8 | 7.2 | 39.9 | 589 | 5.9 | 1.31 | 16.8 | $3.4x10^5$ |
| $k_{01}/\alpha_1$=62/0.032 | 27.6 | 6.9 | 21.3 | 791 | 5.9 | 0.98 | 14.2 | $3.0x10^5$ |
| $k_{02}/\alpha_2$=38/0.021 | 34.5 | 6.6 | 18.4 | 988 | 5.8 | 0.78 | 14.8 | $2.3x10^5$ |
| | 51.7 | 6.4 | 12.8 | 1250 | 5.8 | 0.62 | 13.9 | $2.0x10^5$ |
| **V-9** | 3.5 | 2.0 | 3.10 | 962 | 0.68 | 1.32 | 5.98 | $6.2x10^5$ |
| | 6.9 | 1.8 | 2.55 | 1050 | 0.59 | 1.21 | 5.66 | $6.0x10^5$ |
| $\tau/\phi_{ST}$=3.6/0.6 | 13.8 | 1.7 | 1.71 | 1290 | 0.72 | 0.98 | 5.14 | $5.4x10^5$ |
| $k_{01}/\alpha_1$=3.8/0.058 | 27.6 | 1.4 | 0.76 | 2020 | 0.77 | 0.63 | 4.31 | $4.1x10^5$ |
| | 34.5 | 1.3 | 0.514 | 2470 | 0.79 | 0.51 | 3.90 | $3.7x10^5$ |
| | 51.7 | 0.3 | 0.190 | 4090 | 0.00 | 0.31 | 3.05 | $2.9x10^5$ |

**Table 2b.** Measured (k, $\phi_E$, F) and derived ($\phi_S$, $\phi_C$, $d_C$, $n_C$) parameters for two shale samples from the Beaufort–Mackenzie Basin (northern Canada; Katsube et al. (1996b, 1999b)) and one seafloor sample from offshore Nova Scotia (Katsube and Coyner, 1994; Loman et al., 1993).

| Sample | $P_E$ (MPa) | $\phi_E$ (%) | k ($x10^{-21} m^2$) | F | $\phi_S$ (%) | $\phi_C$ (%) | $d_C$ (nm) | $n_C$ ($/m^2$) |
|---|---|---|---|---|---|---|---|---|
| **B-TG-6b** | 3.5 | 12.2 | 258 | 166 | 9.0 | 3.19 | 22.7 | $7.5x10^5$ |
| | 6.9 | 12.2 | 126 | 185 | 9.3 | 2.86 | 16.8 | $9.1x10^5$ |
| $\tau/\phi_{ST}$=1.9/9.1 | 13.8 | 11.1 | 29.5 | 250 | 9.0 | 2.12 | 9.41 | $1.2x10^6$ |
| $k_{01}/\alpha_1$=540/0.212 | 27.6 | 10.3 | 5.65 | 447 | 9.1 | 1.19 | 5.50 | $1.1x10^6$ |
| $k_{02}/\alpha_2$=23/0.051 | 34.5 | 10.0 | 3.97 | 668 | 9.2 | 0.79 | 5.64 | $7.5x10^5$ |
| | 51.7 | 9.5 | 1.65 | 1308 | 9.1 | 0.41 | 5.09 | $4.2x10^5$ |
| **EJA-2** | 3.5 | 33 | 109 | 12.4 | 21.2 | 12.1 | 4.02 | $3.0x10^7$ |
| | 6.9 | 32 | 52.5 | 16.8 | 22.7 | 8.92 | 3.25 | $2.9x10^7$ |
| $\tau/\phi_{ST}$=1.0/24.2 | 13.8 | 30 | 25.5 | 20.9 | 22.9 | 7.18 | 2.53 | $2.8x10^7$ |
| $k_{01}/\alpha_1$=230/0.214 | 27.6 | 29 | 19.4 | 25.1 | 23.1 | 5.98 | 2.42 | $2.5x10^7$ |
| $k_{02}/\alpha_2$=57/0.055 | 34.5 | 27 | 8.69 | 39.4 | 23.4 | 3.81 | 2.03 | $1.9x10^7$ |
| | 51.7 | 25 | 3.86 | 76.8 | 23.4 | 1.96 | 1.88 | $1.0x10^7$ |
| **VSF-1** | 1 | 46 | 443 | 6.15 | 16.0 | 30.1 | 5.72 | $4.7x10^7$ |
| | 2 | 42 | 325 | 6.59 | 14.3 | 28.0 | 5.07 | $5.0x10^7$ |
| $\tau/\phi_{ST}$=1.11/0.72 | 3 | 39 | 223 | 7.06 | 12.8 | 26.2 | 4.35 | $5.4x10^7$ |
| $k_{01}/\alpha_1$=660/0.373 | 4 | 36 | 157 | 7.57 | 11.5 | 24.4 | 3.78 | $5.8x10^7$ |
| $k_{02}/\alpha_2$=76/0.028 | 5 | 33 | 97 | 8.11 | 10.2 | 22.8 | 3.07 | $6.7x10^7$ |
| | 7 | 28 | 60 | 9.31 | 8.1 | 19.9 | 2.59 | $6.9x10^7$ |

$P_E$=Effective pressure (confining pressure minus pore pressure)
$\phi_E$=Effective porosity
k=Permeability
F=Formation factor
$\phi_S$=Storage porosity derived by Equations (1) and (3)
$\phi_C$=Connecting porosity
$d_C$=Flow-path size
$n_C$=Flow-path density (tubular) or connecting-pore density
$\tau$=Tortuosity
$\phi_{ST}$=Storage porosity (in per cent) derived from Equation (6)
$k_{01}$, $k_{02}$=Permeability coefficients ($x10^{-21} m^2$) for Equation (7)
$\alpha_1$, $\alpha_2$=Coefficients for Equation (7)

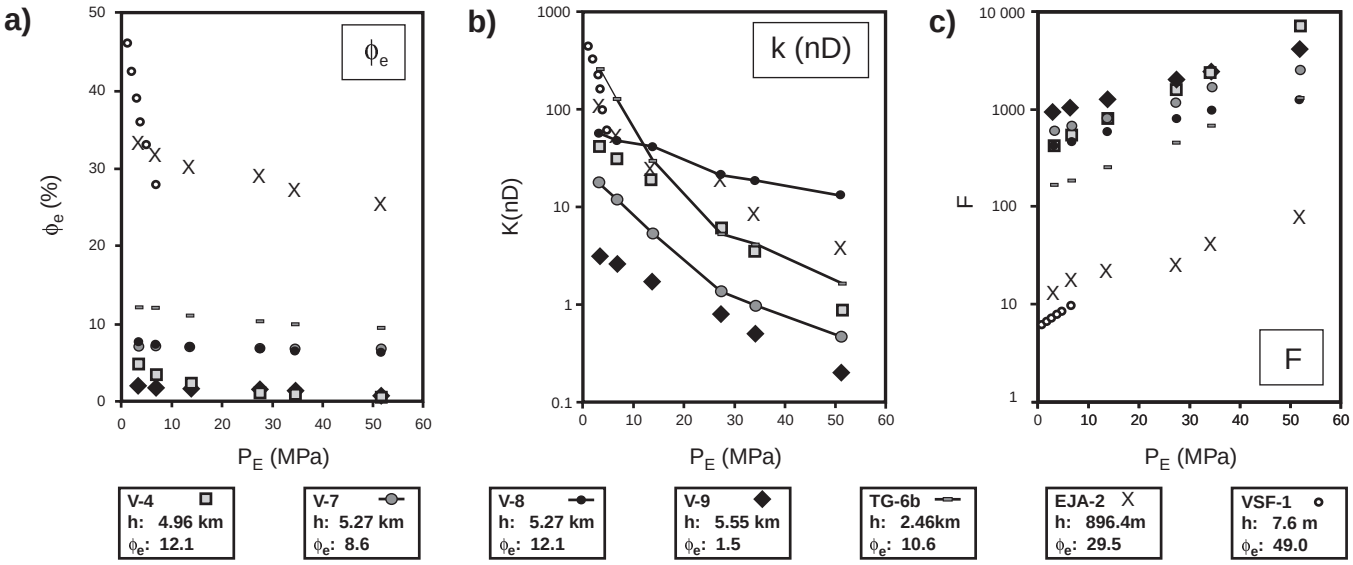


***Figure 3.*** *Pressure (P) characteristics of* ***a)*** *effective porosity ($\phi_E$),* ***b)*** *permeability (k) and* ***c)*** *formation factor (F) for five shale (V-4, V-7, V-8, V-9, TG-6), a mudstone (EJA-2) and a seafloor mud (VSF-1) samples from various depths (0.9–5.3 km) in the Venture Gas Field (VGF; eastern Canada, Katsube and Coyner (1994)) and the Beaufort-Mackenzie Basin (BMB; northern Canada, Katsube et al. (1996b, 1999b)).*

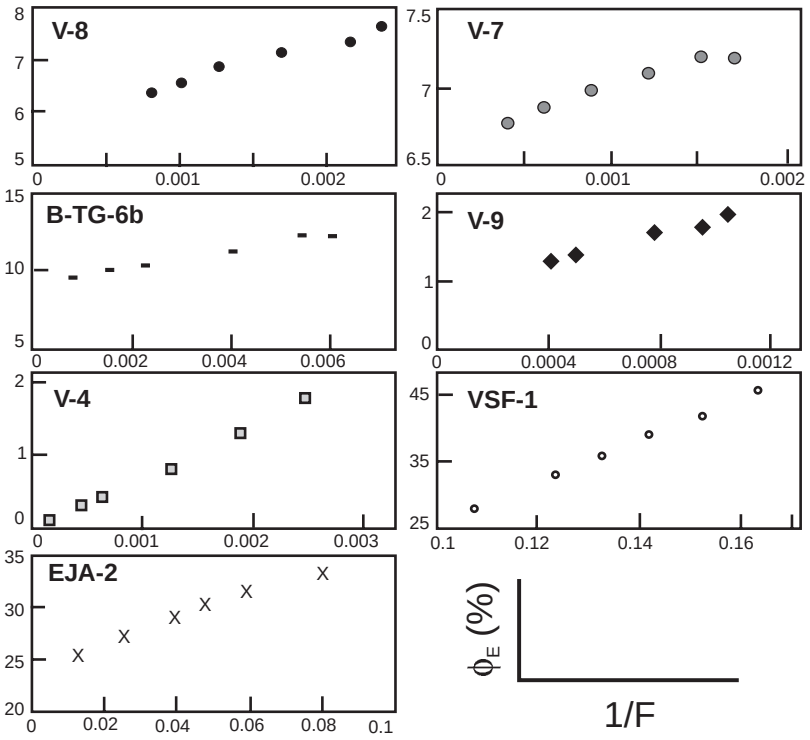


***Figure 4.*** *Effective porosity ($\phi_E$) as a function of the reciprocal of true formation factor (1/F) at different confining pressures, for the same seven samples displayed in Figure 3. The $\tau$ and $\phi_s$ are the tortuosity and storage porosity, respectively.*

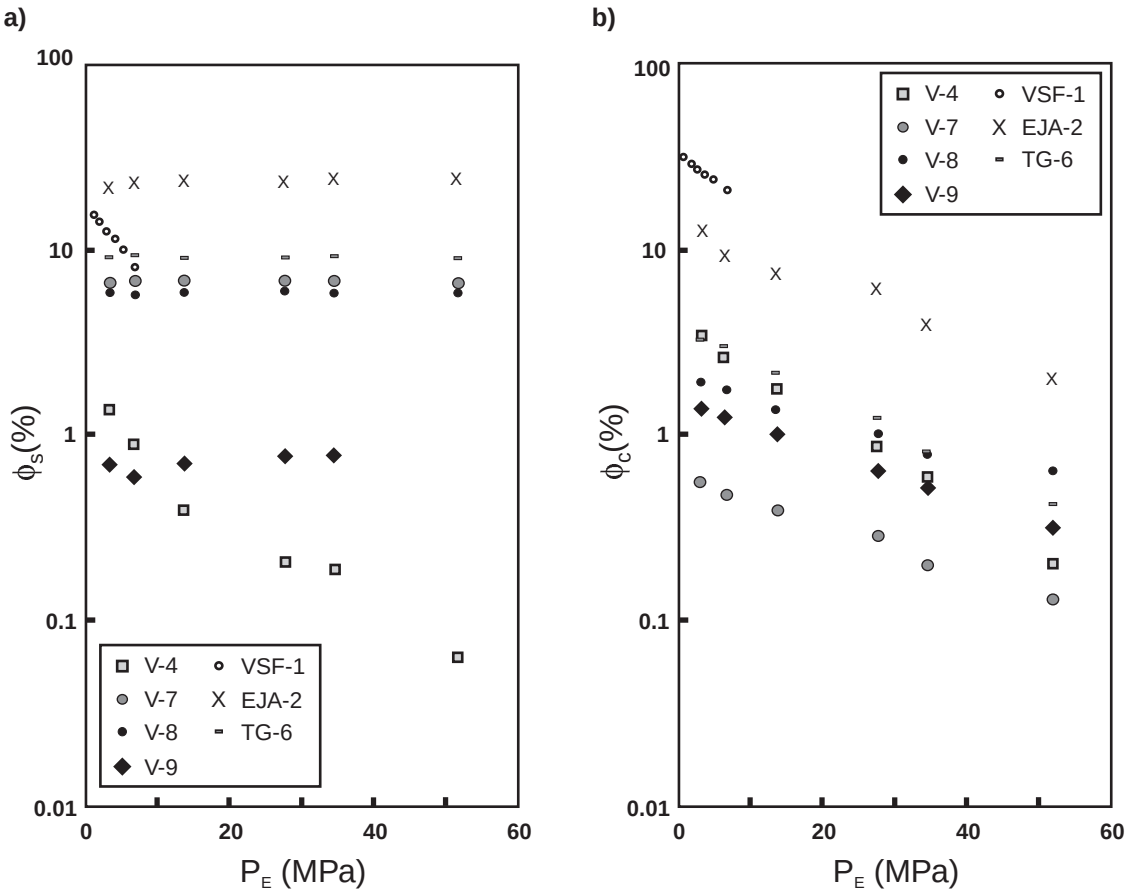


***Figure 5.*** *Pressure (P) characteristics of* ***a)*** *storage porosity ($\phi_S$) and* ***b)*** *connecting porosity ($\phi_C$), for the same seven samples displayed in Figure 3.*

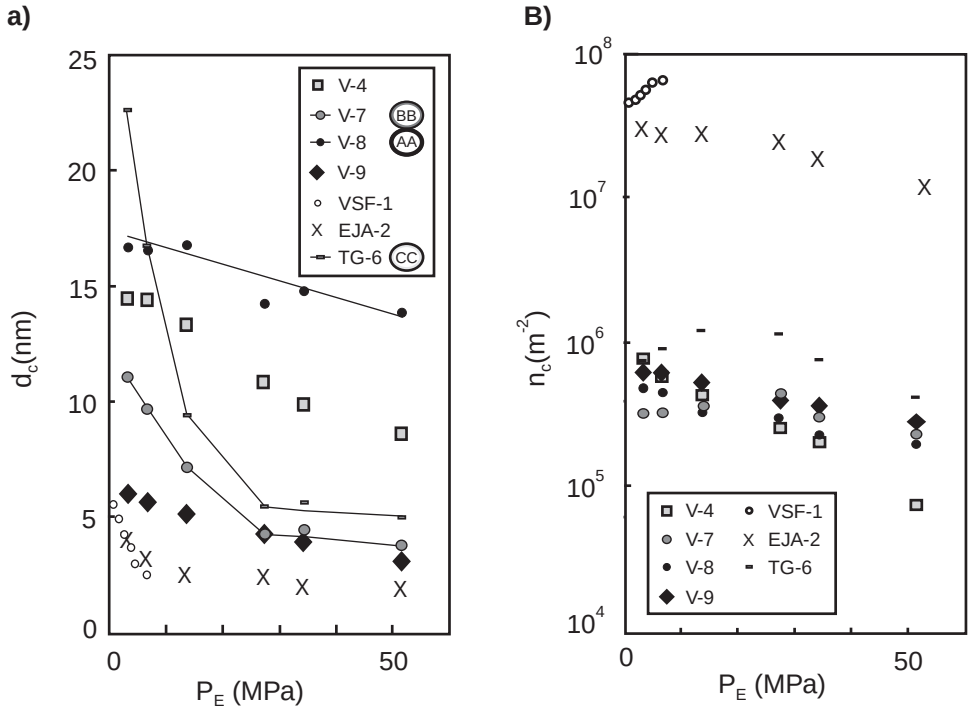


***Figure 6.*** *Pressure (P) characteristics of* ***a)*** *flow-path size ($d_C$), and* ***c)*** *flow-path density ($n_C$), for the same seven samples displayed in Figure 3.*

## DISCUSSION

The curves for storage porosity as a function of effective pressure ($\phi_S$-$P_E$) indicate that $\phi_S$ is generally constant with increased $P_E$, except for two samples (VSF-1, V-4) which show decreased $\phi_S$ with pressure (Fig. 5a). Contrary to that trend, however, the curves for connecting porosity versus effective pressure ($\phi_C$-$P_E$) show decreased $\phi_C$ with increased $P_E$ for all seven samples (Fig. 5b).

The $\phi_S$ decreasing trend with increased $P_E$ for sample VSF-1 is expected, since it is loose seafloor material being compacted for the first time; however, the same trend for sample V-4 is surprising, since it is solid material from a depth of 4.96 km (Table 1). This may be an example of collapsing storage pores due to weakened framework, a model proposed (Katsube et al., 1999a) for shales at an advanced stage of diagenetic dissolution (Katsube and Williamson, 1994). The trend of little to no $\phi_S$ variation with increased $P_E$ is expected, since these shale and mudstone samples (V-7, V-8, V-9, B-TG-6) are either at a state of maximum compaction (burial depth >2.5–3.5 km), framework supported, or an advanced stage of diagenetic cementation (Katsube and Williamson, 1994, 1998; Bloch and Issler, 1996); however, the same trend for sample EJA-2 is surprising, since this mudstone is unaltered from a depth of 0.9 km (Table 1), a depth normally not expected to have reached state of maximum compaction. A separate study (Katsube et al., 1999b) suggest that it is framework supported. The fact that the $\phi_C$-$P_E$ curves for all samples show considerable $\phi_C$ decrease with increased $P_E$, suggests that connecting pores are considerably more flexible than storage pores, regardless of their texture. This implies that the connecting pores are more susceptible to changes in pore or effective pressures.

The flow-path size versus effective pressure ($d_C$-$P_E$) curves show considerable $d_C$ decrease with increased $P_E$ (Fig. 6a). The vary rapid decrease for some samples (V-7, B-TG-6, VSF-1, EJA-2) at lower pressures ($P_E$<20–30 MPa), reflects the closing of destressed pores resulting from removing samples from their in situ condition (Katsube and Coyner, 1994; Best and Katsube, 1995). The k-$P_E$ curves, typified by those of samples V-8, V-7, and B-TG-6 (Fig. 3b, 6a) representing groups AA, BB, and CC (Katsube and Connell, 1998), strongly resemble those of $d_C$-$P_E$ as is expected (Equation (4)). The $d_C$ values at the maximum $P_E$ values are 1.5–11 nm. Many of the flow-path density versus effective pressure ($n_C$-$P_E$) curves, surprisingly, show increased $n_C$ or an increase followed by a decrease with increased $P_E$ (Fig. 6c). The model offered to explain this trend is closing of sheet-like connecting pores with rough irregular surfaces. When such sheet-like pores close, the two irregular surfaces will make many point contacts but not form a complete closure, resulting in an increased number of smaller pores.

The $\phi_S$-$P_E$ curves for samples VSF-1 and V-4, showing clear $\phi_S$ decreases with increased pressure (Fig. 5a), are contrary to Equation (6) which assumes $\tau$ and $\phi_S$ are constant. An explanation offered for this inconsistency is that their $\phi_E$-1/F curves (Fig. 4) are actually slightly nonlinear, but are being interpreted as linear (constant $\tau$), resulting in $\phi_S$ being variable when calculated, using Equations (1) and (3).

## CONCLUSIONS

This study has shown that, although some theoretical problems still exist, the pressure characteristics can be successfully determined for shale and mudstone storage ($\phi_S$) and connecting ($\phi_C$) porosities. Although some show a $\phi_S$ decrease with increased effective pressure ($P_E$), $\phi_S$ is generally constant with pressure. Contrary to that, $\phi_C$ always shows a considerable decrease with increased pressure, suggesting that connecting pores are more flexible than storage pores and are more susceptible to pore-pressure changes. The flow-path size ($d_C$) data show considerable decrease with increased pressure, displaying values of 1.5–11 nm at the maximum pressures ($P_E$ =50–60 MPa ) used in this study.

## ACKNOWLEDGMENTS

The author expresses sincere thanks to S. Connell (Geological Survey of Canada) for preparing the diagrams and part of the data contained in this paper. The author expresses sincere appreciation to G.L. Bowers (Applied Mechanics Technologies, Houston, Texas, U.S.A.) for the critical review of this paper and for the advice and useful comments on this study.

## REFERENCES

**Best, M.E. and Katsube, T.J.**
1995: Shale permeability and its significance in hydrocarbon exploration; The Leading Edge, March, p. 165–170.

**Bloch, J. and Issler, D.R.**
1996: Petrographic and geochemical analyses of Beaufort-Mackenzie Basin shales; Geological Survey of Canada, Open File 3220, 95 p.

**Brace, W.F., Walsh, J.B., and Frangos, W.T.**
1968: Permeability of granite under high pressure; Journal of Geophysical Research, v. 73, p. 2225–2236.

**Coyner, K., Katsube, T.J., Best, M.E., and Williamson, M..**
1993: Gas and water permeability of tight shales from the Venture Gas Field, offshore Nova Scotia; *in* Current Research, Part D; Geological Survey of Canada, Paper 93-1D, p. 129–136.

**Hedberg, H.D.**
1936: Gravitational compaction of clays and shales; American Journal of Science, v. 31, no. 184, p. 241–287.

**Hermanrud, C., Teige, G.M.G., Vik, E., Wensaas, L., and Nordgard Bolas, H.M.**
1999: Overpressure in shales - do we know what they are and why they are there?; *in* Overpressure in Petroleum Exploration, (ed.) A. Mitchell and D. Grauls; Proceedings of Workshop, Pau, France, April 1998; Elf Exploration Production, Memoir 22, p. 43–48.

**Hermanrud, C., Wensaas, L., Teige, G.M.G., Nordgard Bolas, H.M., Hansen, S., and Vik, E.**
1998: Shale porosities from well logs on Haltenbanken (offshore Mid-Norway) show no influence of overpressuring; *in* Abnormal Pressures in Hydrocarbon Environments, (ed.) B.E. Law, G.F. Ulmishek, and V.I. Slavin; American Association of Petroleum Geologists, Memoir 70, p. 65–85.

**Hinch, H.H.**
1980: The nature of shales and the dynamics of hydrocarbon expulsion in the Gulf Coast Tertiary section; AAPG Publication (ISBN: 0-89181-014-5), p. 1–18.

**Issler, D.R. and Katsube, T.J.**
1994: Effective porosity of shale samples from the Beaufort-MacKenzie Basin, northern Canada; *in* Current Research, Part B; Geological Survey of Canada, p. 19–26.

**Katsube, T.J.**
1981: Pore structure and pore parameters that control the radionuclide transport in crystalline rocks; *in* Proceedings of the Technical Program, International Powder and Bulk Solids Handling and Processing, Rosemount, Illinois, May 12–14, 1981, p. 394–409.
1992: Statistical analysis of pore-size distribution data of tight shales from the Scotian Shelf; *in* Current Research, Part E; Geological Survey of Canada, Paper 92-1E, p. 365–372.
1999: True formation factor determination by nonlinear curve fitting; *in* Current Research 1999-D; Geological Survey of Canada, p. 27–34.

**Katsube, T.J. and Collett, L.S.**
1975: Electromagnetic propagation characteristics of rocks; *in* The Physics and Chemistry of Rocks and Minerals, (ed.) R.G.J. Strens; John Wiley & Sons Ltd., London, United Kingdom, p. 279–295.

**Katsube, T.J. and Connell, S.**
1998: Shale permeability characteristics; *in* Current Research 1998-E; Geological Survey of Canada, p. 183–192.

**Katsube, T.J. and Coyner, K.**
1994: Determination of permeability(k)-compaction relationship from interpretation of k-stress data for shales from Eastern and Northern Canada; *in* Current Research 1999-D; Geological Survey of Canada, p. 169–177.

**Katsube, T.J. and Kamineni, D.C.**
1983: Effect of alteration on pore structure of crystalline rocks: core samples from Atikokan, Ontario; Canadian Mineralogist, v. 21, p. 637–646.

**Katsube, T.J. and Mareschal, M.**
1993: Petrophysical model of deep electrical conductors; graphite lining as a source and its disconnection due to uplift; Journal of Geophysical Research, v. 98, no. B5, p. 8019–8030.

**Katsube, T.J. and Williamson, M.A.**
1994: Effects of diagenesis on shale nano-pore structure and implications for sealing capacity; Clay Minerals, v. 29, p. 451–461.
1998: Shale petrophysical characteristics: permeability history of subsiding shales; *in* Shales and Mudstones II, (ed.) J. Schiber, W. Zimmerle, and P.S. Sethi; Stattgard, Germany, p. 69–91.

**Katsube, T.J., Best, M.E., and Mudford, B.S.**
1991: Petrophysical characteristics of shales from the Scotian shelf; Geophysics, v. 56, p. 1681–1688.

**Katsube, T.J., Bloch, J., and Cox, W.C.**
1999a: The effect of diagenetic alteration on shale pore-structure and its implications for abnormal pressures and geophysical signatures; *in* Overpressure in Petroleum Exploration (ed.) A. Mitchell, and D. Grauls; Proceedings of Workshop Pau, France, April 1998; Elf Exploration Production, Memoir 22, p. 49–54.

**Katsube, T.J., Boitnott, G.N., Lindsay, P.J., and Williamson, M.**
1996a: Pore structure evolution of compacting muds from the seafloor, offshore Nova Scotia; *in* Current Research 1996-D; Geological Survey of Canada, p. 17–26.

**Katsube, T.J., Dallimore, S.R., Uchida, T., Jenner, K.A., Collett, T.S., and Connell, S.**
1999b: Petrophysical environment of sediments hosting gas-hydrate, JAPEX/JNOC/GSC Mallik 2L-38 gas hydrate research well; *in* Scientific Results from JAPEX/JNOC/GSC Mallik 2L-38 Gas Hydrate Research Well, Mackenzie Delta, North West Territories, Canada: (ed.) S.R. Dallimore, T. Uchida, and T.S. Collett; Geological Survey of Canada, Bulletin 544, p. 109–124.

**Katsube, T.J., Issler, D.R., and Coyner, K.**
1996b: Petrophysical characteristics of shale from the Beaufort-MacKenzie Basin, northern Canada: permeability, formation factor, and porosity versus pressure; *in* Current Research 1996-B; Geological Survey of Canada, p. 45–50.

**Loman, J.M., Katsube, T.J., Correia, J.M., and Williamson, M.A.**
1993: Effect of compaction on porosity and formation factor for tight shales from the Scotian Shelf; *in* Current Research, Part E; Geological Survey of Canada, Paper 93-1E, p. 331–335.

**Magara, K.**
1980: Comparison of porosity-depth relationships of shale and sandstone; Journal of Petroleum Geology, v. 3, p. 175–185.

**Walsh, J.B. and Brace, W.F.**
1984: The effect of pressure on porosity and the transport properties of rocks; Journal of Geophysical Research, v. 89, p. 9425–9431.

**Wardlaw, N.C. and Taylor, R.P.**
1976: Mercury capillary pressure curves and the interpretation of pore structure and capillary behaviour in reservoir rocks; Bulletin of Canadian Petroleum Geology, v. 24, p. 225–262.

Geological Survey of Canada Project 870057